Decoding Protein Gas-Phase Stability with Alanine Scanning and Collision-Induced Unfolding Ion Mobility Mass Spectrometry

Jeddidiah Bellamy-Carter,*[a] Louisa O'Grady,[a] Munro Passmore,[b] Matthew Jenner,[b,c] and Neil J. Oldham*[a]

[a] Dr. J. S. G. Bellamy-Carter, L. O'Grady, Prof. N.J. Oldham
School of Chemistry
University of Nottingham
University Park, Nottingham, NG7 2RD (UK)
E-mail: j.s.g.bellamy-carter@bham.ac.uk, neil.oldham@nottingham.ac.uk
[b] M. Passmore, Dr. M. Jenner
Department of Chemistry
University of Warwick
Coventry, CV4 7AL (UK)
[c] Dr. M. Jenner
Warwick Integrative Synthetic Biology Centre
University of Warwick
Coventry, CV4 7AL (UK)

Supporting information for this article is given via a link at the end of the document.

Abstract: Native mass spectrometry is a widely used tool in structural biology, providing information on protein structure and interactions through preservation of complexes in the gas-phase. Herein, the importance of intramolecular non-covalent interactions in the gas-phase has been studied by alanine scanning and collision-induced unfolding (CIU) ion mobility-mass spectrometry. Mutation of specific polar and ionic residues on the surface of an acyl carrier protein (ACP) were found to destabilise the compact gas-phase structure with mutants E31A, D32A, D41A and D65A being particularly destabilised. Molecular dynamics simulations of the ACP 7+ and 8+ ions showed extended intramolecular interactions, resulting from sidechain collapse of polar surface residues, which were confined to the gas-phase and consistent with the CIU data. These findings provide evidence for the importance of specific ionic residues, and their interactions, in the maintenance of compact protein gas-phase structure.

Introduction

Native mass spectrometry (nMS) is now widely used to address questions in structural biology.[1,2] Probing protein–protein interactions (PPIs) and protein–ligand interactions is the mainstay of nMS,[2–4] with many non-covalent complexes being preserved in the gas-phase environment of the mass spectrometer. Initially controversial, it is generally accepted that the 'native-like' structure of proteins in the gas-phase is broadly reflective of that in solution when sufficiently gentle conditions are applied.[3,5] There are some caveats, however. Firstly, the non-polar (ε_{rel} = 1)[6] high-vacuum environment of the mass spectrometer is believed to cause external polar and ionic amino-acid sidechains to collapse back onto the protein's surface to provide charge solvation.[7] Secondly, the net charge of protein ions produced by electrospray ionisation (ESI) is often quite different from that in solution. In the former, the net charge is determined by Coulomb repulsion and distribution of individual residues across the surface area of the protein ion, whilst in the latter charge is determined by a combination of the pK_a of each ionizable functional group and the solution pH. Ionic interactions are dominant in the gas-phase, and may be the principal driving force for structural stabilisation.[8–11] While kinetically trapped, partially collapsed gas-phase protein ions can remain unperturbed for many milliseconds,[12] which is typically longer than the time from desolvation to detection in a nMS measurement. Activation of the ions[13] can lead to gross structural rearrangement, and eventually results in the protein ion unfolding, with the neutral and hydrophobic sidechain residues exposed to the vacuum.

A number of techniques exist to probe gas-phase protein structure and interactions, including but not limited to: electron capture dissociation (ECD),[14,15] UV photodissociation (UVPD),[16] infrared spectroscopy,[10,17] gas-phase hydrogen–deuterium exchange (HDX)[18] and ion mobility spectrometry (IMS). The mobility of an ion travelling through an electric field is a function of its charge and collisional cross-section (CCS). Ion mobility–mass spectrometry (IM–MS) allows gas-phase ions to be separated according to CCS-to-charge and mass-to-charge, giving two-dimensional data.[19,20] CCS allows information about the folded status of protein ions to be inferred, and compared with gas-phase molecular dynamics (MD) simulations.[21–25] In many cases, IM–MS has been combined with the UVPD, HDX and MD, among others, to obtain multiplexed information.[16,18,21–23] The combination of IM–MS with collisional activation of protein ions, prior to ion mobility separation, is referred to as collision-induced unfolding (CIU).[12,13,26–31] This technique can be used to analyse and compare the stability of compact protein ions in the gas-phase by determining the collision energy required to induce unfolding pathways.

Acyl carrier proteins (ACPs) are a group of structurally homologous proteins found in fatty acid synthases (FASs), polyketide synthases (PKSs) and non-ribosomal peptide synthetases (NRPSs).[32–35] Comprised of four alpha-helices, their function is to tether and transfer the growing natural product intermediate between enzymatic domains via a phosphopantetheine moiety, which is post-translationally appended to a conserved serine residue on the ACP. Although ACPs are structurally homologous, they have low sequence similarity, even within related biosynthetic pathways. With the exception of a conserved hydrophobic core and the conserved phosphopantetheinyl attachment site, the nature of sidechains is highly variable. We propose that such a protein provides a

convenient vehicle to determine the contribution of specific sidechain residues to the stability of a compact gas-phase protein fold.

Herein we report a comparative CIU–IM–MS study on a set of 34 alanine mutants of an ACP from the bacillaene PKS (PksJ ACP4, see Figure S1).[36] We show how mutating certain polar sidechains to alanine causes destabilisation of the compact gas-phase protein structure, and employ MD to rationalise these observations in terms of key gas-phase intramolecular interactions. We also release scripts for determining charge placement (ChargePlacer) on protein ions produced by ESI, which are applicable to *in silico* alanine scanning. This work highlights the importance of specific surface amino-acid sidechains for the preservation of compact protein ions in the gas-phase.

Results and Discussion

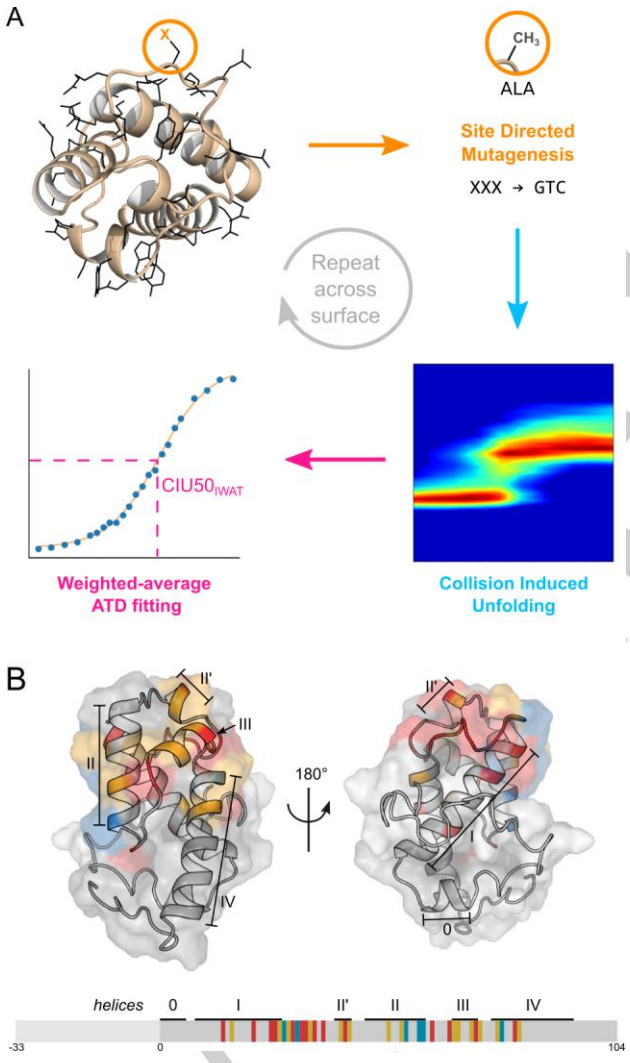

Figure 1. Alanine scanning site-directed mutagenesis of PksJ ACP4. A) Schematic overview of the approach described herein. B) Cartoon representation of PksJ ACP4 with mutated residues (see Table S1 for list of mutants) highlighted according to type: acidic (DE), red; basic (KR), blue; uncharged, yellow. A 2-D map of PksJ ACP4 with mutated residues highlighted. Helices are indicated as black bars and numbering shown.

The overall strategy for the alanine-scanning–CIU approach is summarised in Figure 1A. Systematic replacement of ACP4 amino acids with alanine is followed by CIU to assess the effect of the mutation on the stability of the compact gas-phase protein structure. Individual alanine mutants of PksJ ACP4 were produced using site-directed mutagenesis as described in the Electronic Supporting Information. Mutation of residues in the hydrophobic core yielded insoluble protein, as did mutation of residues neighbouring the conserved phosphopantetheine arm attachment site. In total, 34 soluble alanine mutants were investigated in this study (see Figure 1B and Table S1).

CIU of wildtype PksJ ACP4. The nMS spectra of wildtype PksJ ACP4 consisted of two prominent charges states: 8+ at *m/z* 1903 and 7+ at *m/z* 2175. The protein exhibited approximately 50% *N*-gluconylation (+178 Da) to the N-terminal polyhistidine purification tag[37] and some acetate adduction (Figure S4). The unmodified, purely protonated ions were isolated in the quadrupole region of a Synapt HDMS (Waters) instrument prior to activation in the trap collision cell (see Table S2 for details). No charge stripping or ion fragmentation was observed over the energy range employed in the CIU experiments (Figure S5).

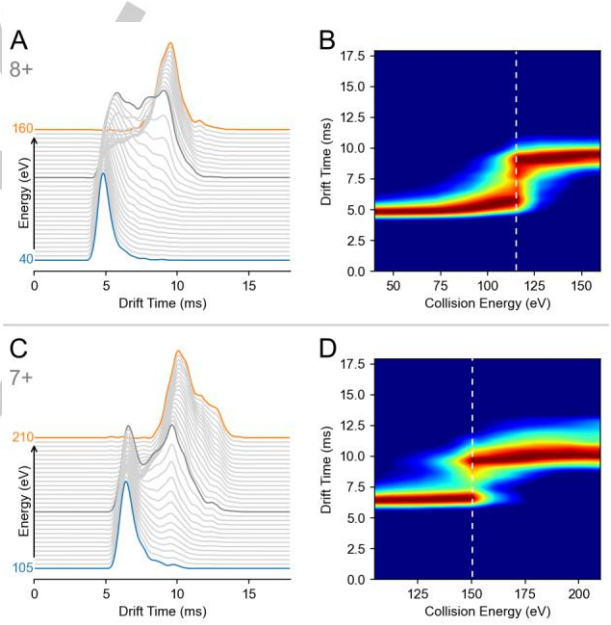

Figure 2. Collision induced unfolding of wildtype PksJ ACP4 for the 8+ (A and B) and 7+ (C and D) charge states, data averaged over 3 replicates. Intensity-averaged arrival time distribution plots, A and C, show the transition from folded (blue) to unfolded (orange) conformers with increasing collision energy (40–160 eV and 105–210 eV for the 8+ and 7+ respectively). The collision energy closest to the CIU50 (116 eV and 150.5 eV respectively) is displayed as a darker grey line. 2D CIU fingerprint plots, B and D, show the single transition between the major compact and unfolded conformations. Fitting curves for all replicates can be seen in Figures S6–S10.

Figure 2 shows IM-MS arrival time distributions (ATDs) (A and C) and 2D CIU plots (B and D) for CIU of wildtype ACP4. Both charge states show a simple, approximately two-state transition occurring at 13–15 V (104–120 eV) and 21–23 V (147–161 eV) for the 8+ and 7+ charge states, respectively. Between these energies, the protein structure unfolded from a dominant compact conformation to a dominant unfolded

conformation. The transition point (50% unfolding, termed CIU50) was determined using both the feature detection (FD) functionality of CIUSuite2[38] and separately fitting the intensity-weighted arrival times (IWAT) with in-house scripts, referred to as $CIU50_{FD}$ and $CIU50_{IWAT}$ hereafter. These values were in broad agreement with each other: 113 ± 2 eV and 114 ± 2 eV for the 8+ charge state and 148 ± 5 eV and 151 ± 4 eV for the 7+ charge state ($CIU50_{FD}$ and $CIU50_{IWAT}$, respectively, n=4 experimental repeats, see Figures S7–S10). For the simple, single transition, unfolding exhibited by ACP4 (with the instrumentation employed) this agreement was an expected result. For proteins possessing more complex unfolding pathways, where multiple transitions are seen, a $CIU50_{FD}$ value for each transition would be determined but only one $CIU50_{IWAT}$ would be obtained, which represents the mid-point for the overall unfolding from most compact to most extended conformations. For comparing broad changes or single transition unfolding events, $CIU50_{IWAT}$ may be advantageous, as it fits all data points on a single, simple function and does not require the identification of transitions between features. $CIU50_{FD}$, in contrast, is preferred where information on individual transitions within a more complex unfolding pathway is required.

CIU of ACP4 mutants. To compare the relative stability of each of the 34 ACP4 X→A mutants, their $CIU50_{FD}$ and $CIU50_{IWAT}$ values were determined and converted to energy differences relative to the wildtype measurements to give $\Delta CIU50_{FD}$ and $\Delta CIU50_{IWAT}$, respectively. Negative ΔCIU50 values indicate a lower energy transition point for the unfolding of the mutant and thus destabilisation of the gas-phase protein compared to the wildtype protein. These values are summarised for both 8+ and 7+ charge states in Figure 3 and Table S5 (fitting plots are presented in Figures S11–S48), for brevity only $CIU50_{IWAT}$ data will be discussed further.

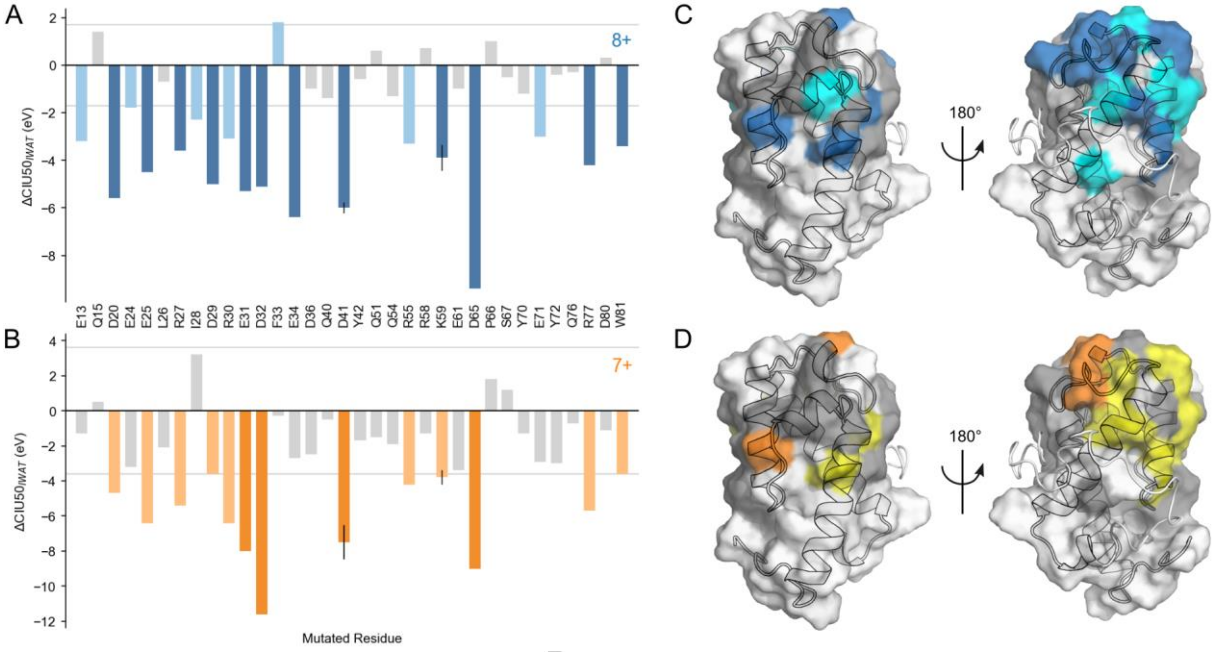

Figure 3. $\Delta CIU50_{IWAT}$ data for ACP4 mutants. Bar plots, A and B, show the $\Delta CIU50_{IWAT}$ values for all ACP4 mutants for the 8+ (A, blue) and 7+ (B, orange) charge states. Grey lines represent one standard deviation (1σ) of the wildtype measurements. Bars are coloured according to the deviation from the wildtype mean: <1σ, grey; >1σ, light shade; >2σ, dark shade. For D41A and K59A mutants error bars indicate the representative standard deviation of the $CIU50_{IWAT}$ measurements (n=3). C and D) Surface representations, with underlaid cartoon outlines, of ACP4 with residues coloured according to $\Delta CIU50_{IWAT}$ deviation from the wildtype mean for the 8+ (C, blue) and 7+ ions (D, orange) as above. This shows that residues causing destabilisation when mutated to alanine are well distributed across the available surface of mutated residues.

The extent of destabilisation was determined by comparing the $\Delta CIU50_{IWAT}$ for each mutant to the standard deviation of the wildtype $CIU50_{IWAT}$ measurements, where values greater than 1σ and 2σ were termed weakly destabilised and strongly destabilised, respectively (see Figure 3). Because of the large number of CIU measurements required to plot unfolding and determine the $CIU50_{IWAT}$ of each mutant reliably (23 and 21 measurements per mutant, for 8+ and 7+ respectively), and our desire to sample a large number of ACP4 mutants, it was not practical to measure every variant in triplicate. Repeat measurements of wildtype ACP4 provided an estimation of the error in $CIU50_{IWAT}$, as reported above. This was judged as an upper estimate, given that the replicates used for error estimation were carried out over five weeks with the potential for drift in instrument conditions. To assess the typical error in $CIU50_{IWAT}$ for the mutants, triplicates of D41A and K59A ACP4 were acquired. Deviations (1σ) of 0.23 and 0.99 eV for the D41A mutant (8+ and 7+, respectively), and 0.55 and 0.40 eV for the K59A mutant (8+ and 7+, respectively) were obtained (error bars shown on Figure 3A–B), which showed statistically significant differences by t-test to the wildtype (p-values of D41A: 0.003 and 0.019, and K59A: 0.0132 and 0.092, for 8+ and 7+ respectively). Further, to ensure the reliability and significance of $\Delta CIU50_{IWAT}$ values, the wildtype protein was repeatedly measured as a standard zero-point $\Delta CIU50_{IWAT}$ throughout the course of CIU data acquisition for the mutants. This meant that

although $CIU50_{IWAT}$ may vary over time, $\Delta CIU50_{IWAT}$ was comparable between variants.

Mutation of many of the acidic and basic residues resulted in destabilisation of the protein in the gas-phase, as measured by negative $\Delta CIU50_{IWAT}$ values. Largest effects were seen with E31A, D32A, D41A and D65A, across both charge states. There were, however, a number of exceptions, namely D36A, R58A, E61A and D80A, indicating that removal of an acidic or basic residue did not—as a matter of course—induce destabilisation. Additionally, mutation of some hydrophobic residues, notably W81A, destabilised the protein. Interestingly, E34A showed significant destabilisation in the 8+ charge state, but not the 7+, otherwise broadly similar effects were seen in both charge states across the mutants examined.

In order to provide structural interpretation of these experimental results, molecular dynamics (MD) simulations were performed on ACP4 ions. Although no high-resolution structure of ACP4 itself is currently available, the highly conserved nature of the ACP fold, and the existence of numerous high-resolution examples in the protein data bank (PDB), made the production of a sufficiently reliable and accurate homology model possible (see Supporting Information for experimental details).

Molecular dynamics on ACP4. Placement of charges for gas-phase simulations of protein ions produced by ESI is non-trivial. Early gas-phase protein MD typically assumed that the acidic sidechains would be neutralised due to their high gas-phase proton affinity (~1450 kJ/mol, see Table S4),[39] but it is now believed that zwitterionic interactions are prevalent in the gas-phase,[40–43] and play an important role in stabilisation. Recently, mobile-proton models for charge calculation during the course of MD simulations have provided a more accurate understanding of charging from the ESI droplet through to microsecond timescales.[23] Point-charge approximations, featuring chargeable sidechains and termini, and more accurate all-atom charge models have both been proposed.[44–46] In order to provide a simple but powerful approach, we developed a freely accessible Python tool, named ChargePlacer, which uses an implementation of the point-charge model for producing protein ions for use in MD simulations. To our knowledge, ChargePlacer is the only downloadable tool specifically designed to interrogate charge placement for gas-phase protein structures and prepare them for MD. Taking inspiration from the algorithm described by Konermann et al.,[23,45,46] ChargePlacer performs a descent by trialling permutations of proton placement (see Figure S3) to reduce the total energy of the system (E_{tot}) accounting for Coulomb repulsion and, optionally, proton affinity (Equation S4). Like the algorithm described by Konermann, ChargePlacer only samples a subset of the permutation space yet this approach yielded reproducible energy-minimised protonation patterns (see Figure S49–S51), which were then used for gas-phase MD simulations of ACP4 ions. The mobility of protons during MD simulations[44–46] is not implemented directly in ChargePlacer, although this could be introduced through supplementary scripting. Uniquely, ChargePlacer also provides *in silico* alanine scanning functionality, which calculates the minimised protonation pattern for each mutation of a chargeable sidechain to alanine (see Figure S52 for this applied to $ACP4^{8+}$). An option to ignore proton affinity in the calculations, is provided, which—for the protein systems tested—generally yielded protonation patterns with more zwitterionic character (systems used were ACP4, lysozyme and transthyretin (TTR), see Figures S49–S51 and Table S6). When applied to ACP4, MD runs of Coulomb-only energy minimised 8+ and 7+ ions resulted in less unfolding under a thermal gradient than equivalent MD runs using a proton affinity corrected charge distribution (see Figure S53).

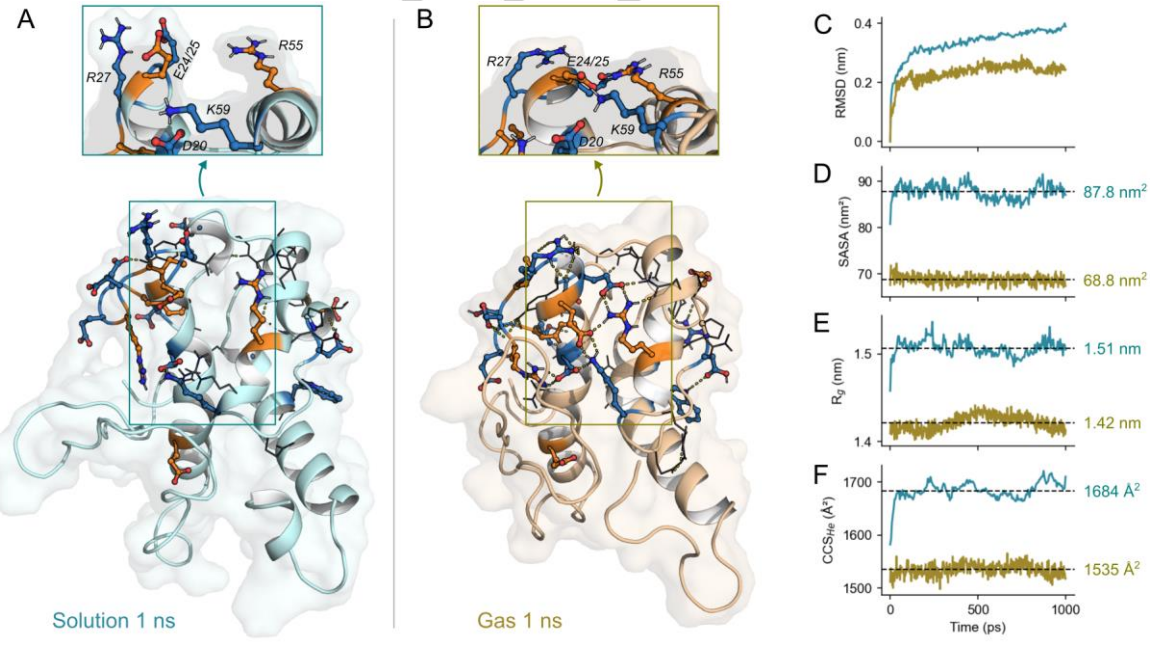

Figure 4. Molecular dynamics simulations of ACP4 at 298 K for 1 ns. Cartoon representations of 1 ns frame for solution-phase (A) and 8+ gas-phase (B) simulations show the relative collapse of polar sidechains, resulting in the reduced size of the gas-phase protein. Zoomed and rotated sections between helices I and II highlight the collapse. Residues mutated to alanine in this study are shown as sticks, and coloured according to $\Delta CIU50_{IWAT}$: ≥1σ, orange; ≥2σ, blue. Polar contacts (as detected in PyMol) are shown as dashed lines. Root-mean squared deviation (RMSD, C), solvent-accessible surface area (SASA, D), radius of

gyration (R_g, E) and theoretical CCS (F) measures comparing the solution and gas-phase simulations (A and B), coloured blue and olive respectively—showing the gas-phase simulation to be consistently smaller and less flexible.

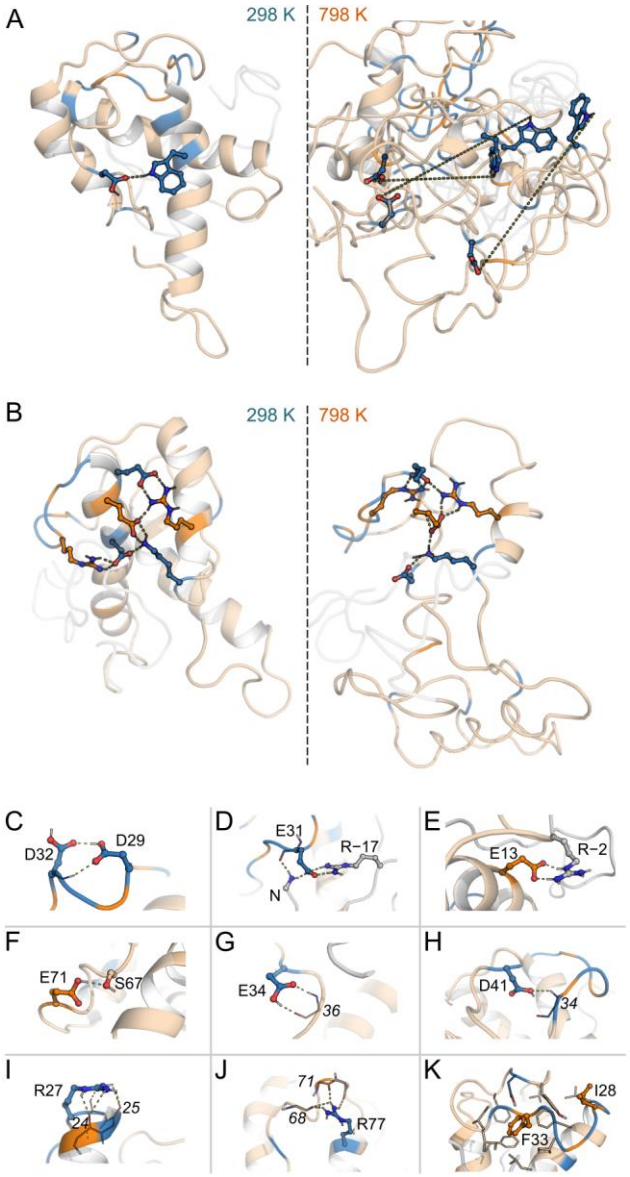

Figure 5. Gas-phase molecular dynamics simulations of the 8+ charge state of ACP4 at room temperature (298 K) and linear thermal gradient (298–798 K) for 1 ns. A) D41–W81 H-bond interaction. B) Extended ionic network involving D20, E24, E25, R30, R55 and K59, bridging helices I and II. C–K) Interactions of other residues that show significant destabilisation, by CIU, when mutated to alanine. Residue sidechains and mainchain atoms are shown as sticks and lines, respectively, and coloured according to $\Delta CIU50_{IWAT}$: ≥1σ, orange; ≥2σ, blue. Polar contacts (as detected in PyMol) are shown as dashed lines.

To assist in the interpretation of the CIU data, gas-phase MD simulations were performed in triplicate on a homology model of wildtype $ACP4^{8+}$ using the charge distribution pattern identified from the ChargePlacer algorithm (Table S8). Simulations were run for 1 ns at 298 K to simulate the nonactivated 'native' gas-phase structure or with a thermal gradient from 298 K to 798 K to induce unfolding; further 4 ns simulations were performed at 798 K to simulate the fully unfolded structure. For comparison, solution-phase MD was also performed for wildtype ACP4 for 1 ns at 298 K. As expected,[7,8] the early stages of the gas-phase simulation at 298 K resulted in polar sidechains collapsing onto the surface of the protein and forming a set of polar bonds and ionic networks (see Figure 4). Solvent accessible surface area (SASA) and radius of gyration (R_g) indicate the compactness of a protein structure and have been shown to correlate with CCS.[19,22] For both measures, the gas-phase MD structures of ACP4 (SASA: 68.8 ± 0.9 nm^2 and R_g: 1.42 ± 0.01 nm) were significantly smaller than their solution-phase counterparts (SASA: 87.8 ± 1.6 nm^2 and R_g: 1.51 ± 0.01 nm), see Figure 4D–E. Theoretically determined CCS values (CCScalc, empirically corrected CCS_{PA}[1]) also show a significant decrease from solution-phase (1684 ± 17 $Å^2$) to gas-phase (1535 ± 11 $Å^2$) structures (Figure 4F).

A notable and reproducible gas-phase interaction observed, was a hydrogen bond between D65 and W81, which bridged helices III and IV, and developed towards the latter stages of the 298 K simulation (shown in Figure 5A) but did not form during the unfolding simulations. This interaction could provide an activation barrier to the unfolding process, albeit by a relatively weak bond, that explains the relative destabilisation of D65A and W81A mutants seen in the CIU experiments. Another feature of the gas-phase ACP4 structure was an extended network involving D20, E24, E25, R30, R55 and K59, which bridged helices I and II (shown in Figure 5B). This interaction was retained throughout the unfolding simulations and went on to form the core of the elongated protein on longer timescales (see Figure S54). Disruption of this extended network would be expected to lower the activation barrier to progressive unfolding, and interestingly the D20A, E24A, E25A, R30A, R55A and K59A mutants had destabilising effects, as measured by their $\Delta CIU50_{IWAT}$ values.

Many of the remaining residues whose mutants showed significant destabilisation of the compact ACP4, measured by CIU (Figure 3), are involved in polar bonding to other sidechains; such as D32 to D29, E31 to G–32 (the N-terminus) and R–17 (residues in the N-terminal affinity tag are given negative numbers to distinguish them from the natural ACP4 residues), E13 to R–2 and E71 to S67 (see Figure 5C–F). Others are involved in H-bonding to protein backbone, such as E34, D41, R27 and R77 (see Figure 5G–H). Interestingly, mutation of the bulky non-polar residue F33 to A (Figure 5K) had a mildly stabilising effect on the 8+ charge state (Figure 3), perhaps by facilitating closer proximity of polar residues on helix I and II. This supports previous hypotheses[40] that new ionic interactions in the gas-phase, not found in solution structures, may form as a result of collisional processes and mutation. Mutation of nearby, but surface exposed, I28 was, in contrast, weakly destabilising for the 8+ charge state, indicating subtle effects in that region. Neither mutation showed significant effects for the 7+ ion, suggesting possible differences in structure between the two charge states. Data from IMS experiments can be more directly compared with MD structures by translating both into CCS units: $^{TW}CCS_{N2\rightarrow He}$ and CCS_{calc}, respectively (see Figures S2 and S55, and Table S3).[1,21,47] The IMS and gas-phase MD data for the 8+ charge state are highly complementary (see Figure S56)—nonactivated $ACP4^{8+}$ (at 40 eV) compares well with the 1 ns

simulation at 298 K, giving weighted-mean experimental and theoretical CCS_{He} values of 1578 Å^2 and 1535 Å^2, respectively. This agreement supports the idea of polar sidechain collapse onto the protein's surface under conditions of minimal gas-phase activation. The extended sidechains of the solution phase simulation, in contrast, lead to a CCS_{He} value of 1684 Å^2. Activated and unfolded ACP4^{8+} (at 160 eV) compares well with the extended 4 ns simulation held at 798 K, giving weighted-mean experimental and theoretical CCS_{He} values of 1949 Å^2 and 1986 Å^2, respectively.

In the solution MD simulation, polar residues remained pointing out into the bulk solvent and did not form the D65–W81 H-bond, the extended ionic network nor the other polar interactions seen in the gas-phase (see Figures 4 and 5). This strongly suggests that the effects observed in these experiments are principally relevant to the gas-phase environment, following sidechain collapse, but the results are also consistent with the absence of gross structural rearrangement upon desolvation.

Charge placement calculations performed for alanine mutants of ACP4^{8+} showed that most mutants adopted slightly altered proton patterns. All those that showed proton displacement had more positive, and therefore less favourable, calculated Coulomb repulsion compared to the wildtype (see Table S7). In each case, the mutated residue was a charge carrier in the wildtype^{8+} and removal resulted in an effective increase in the charge density. Many of the mutants that exhibited experimental destabilisation as measured by CIU were not among these, however, which suggested that the change in global Coulomb repulsion was not an overriding factor for the observed destabilisation, and that removal of the interactions predicted by MD simulations was more significant.

Relevance to the solution-phase. While the focus of this work was to study intramolecular interactions responsible for stabilising the compact structure of ACP4 in the gas-phase, it is interesting to note that several of the important residues identified, namely E25, D41, Y42, D65, E71 and W81, are highly conserved within the sub-group of ACPs to which ACP4 belongs (Figure S57–S60). This sub-group consists of type I PKS ACPs that are immediately upstream of a ketosynthase (KS) within clade XIV of KS phylogeny, these are non-elongating KSs (KS^0) specific for β-hydroxyl substrates.[35,36,48] This ACP–KS^0 pair occurs in the first part of an α,β-double bond generating bimodule; the second part baring a dehydratase (DH) domain.[35] Crucially, these two parts are found on different proteins and require non-covalent PPIs to assemble the PKS. It is likely that these conserved residues in the ACP, as well as those on the KS^0, are involved in these intermolecular interactions—possibly preferentially 'locking' the conformation of the ACP—and that removal of them coincidentally disrupts some prominent intramolecular gas-phase interactions within the ACP, due to their ionic character.

Conclusion

Taking PksJ ACP4 as a simple structural model, we have demonstrated that substitution of polar sidechains (especially acidic and basic ones) with alanine causes destabilisation of compact gas-phase structure measured by CIU. We propose that this effect is caused by the disruption of polar interactions and electrostatic networks that form in the gas-phase. To our knowledge, this is first large-scale probing of protein gas-phase structure combining ASM and CIU. While wholesale ASM is not feasible for many systems, we believe that complementary methods, such as chemical modification of residues, can provide similar insights into the gas-phase protein interactions.

Experimental Section

See the Supporting Information for full experimental details. ASM was performed on singular surface residues with site-directed mutagenesis. CIU was performed on a Synapt G1 HDMS (Waters) from aqueous ammonium acetate. Charge placement was calculated using in-house Python scripts (available at github.com/jbellamycarter/ChargePlacer) and MD performed using GROMACS 5.1.

Acknowledgements

We would like to thank UKRI and the universities of Nottingham and Warwick for funding. MJ is the recipient of a BBSRC Future Leader Fellowship (BB/R01212/1), and MP was supported by the University of Warwick and by the BBSRC through the Midlands Integrative Bioscience Doctoral Training Partnership (BB/M01116X/1). JBC was supported by the BBSRC Doctoral Training Partnership (BB/M008770/1) and the University of Nottingham EPSRC Impact Accelerator Award. We would also like to thank Faculty of Science, University of Nottingham for a PEF award.

Keywords: gas-phase protein structure • ion mobility mass spectrometry • molecular dynamics • noncovalent interactions • protein expression

[1] J. L. Benesch, B. T. Ruotolo, *Curr. Opin. Struct. Biol.* **2011**, *21*, 641–649.
[2] A. C. Leney, A. J. R. Heck, *J. Am. Soc. Mass Spectrom.* **2017**, *28*, 5–13.
[3] B. Ruotolo, C. Robinson, *Curr. Opin. Chem. Biol.* **2006**, *10*, 402–408.
[4] J. A. Loo, *Mass Spectrom. Rev.* **1997**, *16*, 1–23.
[5] B. T. Ruotolo, *Science* **2005**, *310*, 1658–1661.
[6] P. D. Schnier, D. S. Gross, E. R. Williams, *J. Am. Chem. Soc.* **1995**, *117*, 6747–6757.
[7] K. Breuker, F. W. McLafferty, *Proc. Natl. Acad. Sci.* **2008**, *105*, 18145–18152.
[8] K. Breuker, S. Brüschweiler, M. Tollinger, *Angew. Chem. Int. Ed.* **2011**, *50*, 873–877.
[9] M. Schennach, K. Breuker, *Angew. Chem. Int. Ed.* **2014**, *53*, 164–168.
[10] M. K. Drayß, D. Blunk, J. Oomens, N. Polfer, C. Schmuck, B. Gao, T. Wyttenbach, M. T. Bowers, M. Schäfer, *Int. J. Mass Spectrom.* **2009**, *281*, 97–100.
[11] S. Warnke, G. von Helden, K. Pagel, *J. Am. Chem. Soc.* **2013**, *135*, 1177–1180.
[12] S. Myung, E. R. Badman, Y. J. Lee, D. E. Clemmer, *J. Phys. Chem. A* **2002**, *106*, 9976–9982.
[13] K. B. Shelimov, D. E. Clemmer, R. R. Hudgins, M. F. Jarrold, *J. Am. Chem. Soc.* **1997**, *119*, 2240–2248.
[14] R. N. Straus, R. A. Jockusch, *J. Am. Soc. Mass Spectrom.* **2019**, *30*, 864–875.
[15] H. Zhang, W. Cui, M. L. Gross, *Int. J. Mass Spectrom.* **2013**, *354–355*, 288–291.
[16] A. Theisen, R. Black, D. Corinti, J. M. Brown, B. Bellina, P. E. Barran, *J. Am. Soc. Mass Spectrom.* **2019**, *30*, 24–33.

[17] E. N. Kitova, M. Seo, P.-N. Roy, J. S. Klassen, *J. Am. Chem. Soc.* **2008**, *130*, 1214–1226.

[18] U. H. Mistarz, S. A. Chandler, J. M. Brown, J. L. P. Benesch, K. D. Rand, *J. Am. Soc. Mass Spectrom.* **2019**, *30*, 45–57.

[19] A. Konijnenberg, A. Butterer, F. Sobott, *Biochim. Biophys. Acta BBA - Proteins Proteomics* **2013**, *1834*, 1239–1256.

[20] R. Cumeras, E. Figueras, C. E. Davis, J. I. Baumbach, I. Gràcia, *The Analyst* **2015**, *140*, 1376–1390.

[21] M. F. Bush, Z. Hall, K. Giles, J. Hoyes, C. V. Robinson, B. T. Ruotolo, *Anal. Chem.* **2010**, *82*, 9557–9565.

[22] Z. Hall, A. Politis, M. F. Bush, L. J. Smith, C. V. Robinson, *J. Am. Chem. Soc.* **2012**, *134*, 3429–3438.

[23] M. Bakhtiari, L. Konermann, *J. Phys. Chem. B* **2019**, *123*, 1784–1796.

[24] A. Patriksson, E. Marklund, D. van der Spoel, *Biochemistry* **2007**, *46*, 933–945.

[25] D. van der Spoel, E. G. Marklund, D. S. D. Larsson, C. Caleman, *Macromol. Biosci.* **2011**, *11*, 50–59.

[26] J. T. S. Hopper, N. J. Oldham, *J. Am. Soc. Mass Spectrom.* **2009**, *20*, 1851–1858.

[27] J. D. Eschweiler, J. N. Rabuck-Gibbons, Y. Tian, B. T. Ruotolo, *Anal. Chem.* **2015**, *87*, 11516–11522.

[28] S.-J. Hyung, C. V. Robinson, B. T. Ruotolo, *Chem. Biol.* **2009**, *16*, 382–390.

[29] Y. Zhong, L. Han, B. T. Ruotolo, *Angew. Chem. Int. Ed.* **2014**, *53*, 9209–9212.

[30] S. M. Dixit, D. A. Polasky, B. T. Ruotolo, *Curr. Opin. Chem. Biol.* **2018**, *42*, 93–100.

[31] C. Eldrid, J. Ujma, S. Kalfas, N. Tomczyk, K. Giles, M. Morris, K. Thalassinos, *Anal. Chem.* **2019**, *91*, 7554–7561.

[32] D. I. Chan, H. J. Vogel, *Biochem. J.* **2010**, *430*, 1–19.

[33] R. Farmer, C. M. Thomas, P. J. Winn, *PLOS ONE* **2019**, *14*, e0219435.

[34] A. T. Keatinge-Clay, *Nat. Prod. Rep.* **2012**, *29*, 1050.

[35] E. J. N. Helfrich, J. Piel, *Nat. Prod. Rep.* **2016**, *33*, 231–316.

[36] P. D. Straight, M. A. Fischbach, C. T. Walsh, D. Z. Rudner, R. Kolter, *Proc. Natl. Acad. Sci.* **2007**, *104*, 305–310.

[37] D. Schweida, P. Barraud, C. Regl, F. E. Loughlin, C. G. Huber, C. Cabrele, M. Schubert, *J. Biomol. NMR* **2019**, *73*, 71–79.

[38] D. A. Polasky, S. M. Dixit, S. M. Fantin, B. T. Ruotolo, *Anal. Chem.* **2019**, *91*, 3147–3155.

[39] A. Moser, K. Range, D. M. York, *J. Phys. Chem. B* **2010**, *114*, 13911–13921.

[40] R. R. O. Loo, J. A. Loo, *J. Am. Soc. Mass Spectrom.* **2016**, *27*, 975–990.

[41] M. W. Forbes, M. F. Bush, N. C. Polfer, J. Oomens, R. C. Dunbar, E. R. Williams, R. A. Jockusch, *J. Phys. Chem. A* **2007**, *111*, 11759–11770.

[42] Z. Zhang, S. J. Browne, R. W. Vachet, *J. Am. Soc. Mass Spectrom.* **2014**, *25*, 604–613.

[43] J. Li, C. Santambrogio, S. Brocca, G. Rossetti, P. Carloni, R. Grandori, *Mass Spectrom. Rev.* **2016**, *35*, 111–122.

[44] S. K. Fegan, M. Thachuk, *J. Chem. Theory Comput.* **2013**, *9*, 2531–2539.

[45] V. Popa, D. A. Trecroce, R. G. McAllister, L. Konermann, *J. Phys. Chem. B* **2016**, *120*, 5114–5124.

[46] L. Konermann, *J. Phys. Chem. B* **2017**, *121*, 8102–8112.

[47] B. T. Ruotolo, J. L. P. Benesch, A. M. Sandercock, S.-J. Hyung, C. V. Robinson, *Nat. Protoc.* **2008**, *3*, 1139–1152.

[48] T. Nguyen, K. Ishida, H. Jenke-Kodama, E. Dittmann, C. Gurgui, T. Hochmuth, S. Taudien, M. Platzer, C. Hertweck, J. Piel, *Nat. Biotechnol.* **2008**, *26*, 225–233.

WILEY-VCH

Entry for the Table of Contents

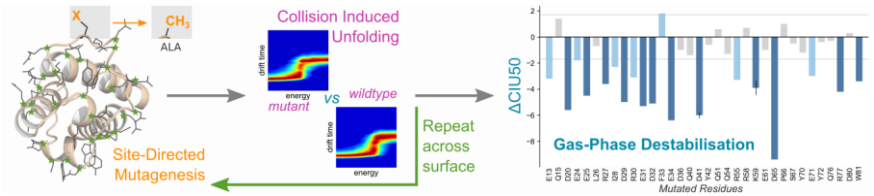

Non-covalent intramolecular interactions of gas-phase proteins can be discovered from differential stability of alanine mutants. Removal of polar and ionic surface residues from proteins, by alanine scanning, destabilises gas-phase protein structures as measured by collision induced unfolding. Molecular dynamics helps to decode interactions disrupted by this removal.

Institute and/or researcher Twitter usernames: @nottschemistry, @warwickchem

WILEY-VCH